CMS Physics Analysis Summary

Contact: cms-pag-conveners-exotica@cern.ch 2011/05/12

Search for Randall-Sundrum Gravitons Decaying into Two Photons in 7 TeV p-p Collisions with the CMS Detector

The CMS Collaboration

Abstract

This note describes the search for Randall-Sundrum gravitons decaying to pairs of photons in the CMS experiment, using 36.1 pb^{-1} of integrated luminosity of proton-proton collisions at $\sqrt{s} = 7$ TeV. We find the diphoton invariant mass spectrum to agree with standard model expectations, and find no evidence for a resonance. We derive limits on the cross-section for the production of Randall-Sundrum gravitons, and hence on the parameters of the warped extra dimension model. For values of the coupling parameter ranging from 0.01 to 0.1, we exclude graviton masses below 371 to 945 GeV/c^2 at the 95% C.L.

New approaches which exploit the geometry of extra spatial dimensions have been proposed to resolve the hierarchy problem of the standard model (SM) [1–6]. The hierarchy problem refers to the large difference between the Planck scale ($M_{Pl} \sim 10^{16}$ TeV) where gravity is expected to be strong, and the scale of electroweak symmetry breaking (~ 1 TeV). The scenario proposed by Arkani-Hamed, Dimopoulos and Dvali (ADD) deals with the case in which the hierarchy is generated by a large volume for the extra dimensions [1, 2]. The Randall-Sundrum (RS) scenario suggests that the observed hierarchy is created by a warped extra dimension [3]. If these theories, in fact, describe the origin of the observed hierarchy, then their signatures should appear at TeV scale experiments.

RS models posit that our universe is described by a higher-dimensional warped geometry. The warping of the extra dimension causes the energy scale of one end of the extra dimension to be much larger than the other end. In the simplest RS model, our universe is represented as a 5-dimensional space, and all particles, except for the graviton, are localized on (3 + 1)-dimensional brane(s). We consider the RS-1 model, which has a finite size for the extra dimension, with two branes, one at each end.

More specifically, the RS-1 model consists of a 5-dimensional non-factorizable geometry based on a slice of AdS_5 space with length πr_c, where r_c is the compactification radius. The metric is given by:

$$ds^2 = e^{-2kr_c y}\eta_{\mu\nu}dx^\mu dx^\nu - r_c^2 dy^2, \tag{1}$$

where the Greek indices extend over ordinary 4-d space, $\eta_{\mu\nu}$ is the metric tensor for Minkowski space-time, and $0 \leq y \leq \pi$ is the coordinate along the single extra dimension of radius r_c. Here k is the AdS_5 curvature scale, or "warp factor", which is of the order of M_{Pl}. The relation between the reduced 4-d Planck scale $\bar{M}_{Pl} \equiv M_{Pl}/\sqrt{8\pi}$, the 5-d Planck scale M_5, the curvature scale k, and the compactification radius r_c is given by:

$$\bar{M}_{Pl}^2 = \frac{M_5^3}{k}(1 - e^{-2kr_c\pi}). \tag{2}$$

The scale of physics phenomena as realized by the 4-d flat metric transverse to the 5th dimension is specified by the exponential warp factor. In this model the scale Λ_3 of any physical processes, as seen on the (3+1)-d flat metric is related to its natural scale Λ by $\Lambda_3 = \Lambda e^{-kr_c\pi}$. As a consequence, the observed hierachy is generated by a geometrical exponential factor in such a way that the scale of the processes we can observe is $\Lambda_\pi = M_{Pl}e^{-kr_c\pi}$. Then, if gravity is localized on the Planck brane, we can naturally obtain TeV scales on the 3-brane at $y = \pi$ if $kr_c \sim 11 - 12$.

In this scenario, gravitons appear as a tower of Kaluza-Klein excitations with masses and widths determined by the parameters of the RS-1 model: the mass of the first graviton excitation mode M_1, and the dimensionless coupling parameter $\tilde{k} \equiv k/\bar{M}_{Pl}$. Precision electroweak data require that $\tilde{k} > 0.01$, while the requirement that the model remains perturbative constrains $\tilde{k} < 0.1$.

The LHC opens a new window in center-of-mass-energy ($\sqrt{s} = 7$ TeV) to detect RS graviton excitations with high resonance masses both for the weak coupling constant $\tilde{k}$=0.01 as well as for the stronger $\tilde{k}$=0.1. This note describes the search for the lowest excitation of RS-1 KK gravitons decaying into diphoton pairs with the CMS detector. The advantage of the diphoton decay channel for the decay of the graviton is the larger branching fraction: 4%, compared to 2% for the e^+e^- and $\mu^-\mu^+$ decay channels.

The most recent and stringent experimental constraints come from $p\bar{p}$ collisions at $\sqrt{s} = 1.96$ TeV at the Tevatron. The CDF experiment has reported a search in the dielectron and diphoton

channel with 5.7 fb^{-1} of data, excluding at the 95% C.L. graviton masses less than $M_1 < 604\ (1055)$ GeV/c^2 at a value of the coupling parameter $k/\overline{M}_{Pl} = 0.01\ (0.1)$ [7, 8]. The D0 experiment presents a search in the dielectron and diphoton channel with 5.4 fb^{-1} of data, excluding at 95% C.L. graviton masses $M_1 < 560\ (1050)$ GeV/c^2 for $k/\overline{M}_{Pl} = 0.01\ (0.1)$ [9].

The Compact Muon Solenoid (CMS) experiment is a general purpose particle detector experiment located at the Large Hadron Collider (LHC) at CERN, in Geneva, Switzerland. The design of the CMS detector centers around a 3.8T iron-core superconducting solenoid. Within the solenoid, at the very heart of the detector, is an all silicon tracker, consisting of 66M pixel and 10M strip detectors. Calorimetry is performed by a high-resolution, high-granularity electromagnetic calorimeter (ECAL), comprised of more than 70k lead-tungstate crystals, and a brass-scintillator hadronic calorimeter (HCAL). The ECAL is divided into two pseudorapidity (η) regions: barrel ($|\eta| < 1.4442$) and endcap ($1.566 < |\eta| < 2.5$). The crystals of the ECAL barrel (EB) are arranged in a projective geometry and have a front face size of approximately 22×22 mm^2, corresponding to a granularity of $\Delta\eta \times \Delta\phi = 0.0174 \times 0.0174$, where ϕ is the azimuthal angle. Just outside the solenoid is a scintillator-based tail-catching hadronic outer calorimeter. In addition, a steel and quartz fibre forward hadronic calorimeter system is placed on both sides of the detector endcaps to ensure hermiticity. The iron yoke of the magnet system is instrumented with a muon spectrometer, composed of three detector technologies: drift tubes in the central region and cathode strip chambers in the endcaps, both complemented by resistive plate chambers. A more detailed description of the CMS Detector can be found elsewhere [10–12].

A data sample recorded by the CMS detector at $\sqrt{s} = 7$ TeV, corresponding to an integrated luminosity of 36.1 pb^{-1}, is used in this analysis. Events were selected only if they are consistent with collision data and have a well-reconstructed primary vertex, as described in [13]. We required that the events selected pass a double photon trigger requiring energy deposits greater than 10, 15, 17, or 22 GeV, depending on the run period. This trigger selection is 100% efficient for events which pass our offline diphoton selection.

The data are compared to a full Monte Carlo simulation based on GEANT4 [14] of PYTHIA6 [15] generated events. Simulated background samples for Born and Box diphoton production, γ+jet, QCD di-jets, and Drell-Yan e^+e^- are used to model the shape of the background distribution in data. The simulated signal samples of RS-1 gravitons, used to estimate the signal efficiency, span from $M_1 = 250$ to 2000 GeV/c^2 in steps of 250 GeV/c^2, with $\tilde{k} = 0.01,\ 0.05,\ 0.10$.

Photon candidates are reconstructed as superclusters in the ECAL; energy depositions are clustered into superclusters, which are extended in ϕ, to recover the energy deposited by bremsstrahlung and photon conversions. Anomalous signals arising from the interaction of neutral particles, either from prompt or secondary interactions, interacting directly with the photo-detectors of the ECAL barrel are removed using shower shape and pulse timing information. The reconstruction of photons with 7 TeV data is detailed further in [16].

The main challenge to identifying true photon candidates arises from hadronic jets which are misidentified as photons. This occurs when the energy of a jet is dominated by a neutral hadron, such as a π^0 or η, which decays into two photons. If the hadron is highly energetic, the two photons from the decay may be difficult to distinguish and can be mis-identified as a single energetic photon. To discriminate against such backgrounds, we utilize various isolation variables. Jets will typically have a larger number of neutral and charged particles reconstructed in their vicinity, and also a larger fraction of hadronic to electromagnetic energy deposited than photons. Likewise, hadronic and electromagnetic deposits arising from jets will be less isolated than for photons. We use in addition shower-shape variables which are sensitive to the pres-

ence of one or more photons in the electromagnetic shower. Throughout this note, p_T refers to the transverse momentum of the photon, for which we require $p_T > 30\,\text{GeV}$. ΔR defines a cone around a photon with coordinates $(\eta_\gamma, \phi_\gamma)$ such that $\Delta R = \sqrt{(\eta - \eta_\gamma)^2 + (\phi - \phi_\gamma)^2}$. The following set of tight criteria are used to identify photons:

- H/E: The ratio of the hadronic energy of all the HCAL hits in a cone of $\Delta R < 0.15$ centered on the photon, to the electromagnetic energy of the photon. We require $H/E < 0.05$.
- ECAL Isolation: ΣE_T of ECAL hits within a cone of $(0.06 < \Delta R < 0.4)$ around the photon. A rectangular strip $\Delta\eta = 0.04$ is removed from the sum to exclude energy lost in conversions. We require ECAL Isolation $< 4.2 + 0.006 \cdot p_T$ GeV.
- HCAL Isolation: ΣE_T of HCAL hits within a cone of $(0.15 < \Delta R < 0.4)$ around the photon. We require HCAL Isolation $< 2.2 + 0.0025 \cdot p_T$ GeV.
- Track Isolation: Σp_T of tracks within a hollow cone $(0.04 < \Delta R < 0.4)$ around the super cluster. A strip $\Delta\eta = 0.015$ is excluded in the sum. We require track isolation $< 2.0 + 0.001 \cdot p_T$ GeV.
- Shower Shape ($\sigma_{i\eta i\eta}$): $\sigma_{i\eta i\eta}$ is the second moment of the cluster about its average η position, $\sigma^2 = \Sigma_i w_i(\eta_i - \bar{\eta})^2 / \Sigma_i w_i$, where $w_i = \max(0, 4.7 + \ln(\mathrm{E_i/E}))$ and i is the index of a crystal in a 5×5 array centered on the highest energy crystal [16]. We require $\sigma_{i\eta i\eta} < 0.013$.
- Track Veto: To ensure that we are not mis-identifying electrons as photons, we also require a veto on the presence of hits in the pixel detector, which would be consistent with a track compatible with the ECAL energy deposition.

Since the jet-faking-photon rates are higher in the endcap region and also because the signal is more centrally produced than the SM backgrounds, the signal-to-background ratio for endcap photons is worse than in the barrel. We thus chose to focus on barrel photons for this preliminary result, requiring $|\eta_\gamma| < 1.4442$.

The signal efficiency is measured using the RS graviton simulation samples described earlier. After applying the kinematic and efficiency requirements described earlier, the resulting acceptance times efficiency for selecting diphoton events varies between $\sim 25 - 55\%$, depending on the M_1 and $\tilde{k}$. Figure 1 shows the diphoton invariant mass spectra for the signal samples, after the selection is applied and scaled to 36.1 pb^{-1}.

We apply a correction to the signal photon efficiency, to account for any difference in efficiency between data and simulation. The correction is derived from a comparison of electron efficiency in simulation to the efficiency measured using the tag-and-probe method with Z^0 decays [17, 18]. For the photon selection applied above, we apply a scale factor of 0.97 ± 0.01 for the single photon efficiency.

The dominant backgrounds to this search arise in the following forms:

- $\gamma\gamma$: Prompt SM diphoton production from quark annihilation ("Born") and gluon fusion ("Box") processes. With the same final state as our signal, these are an intrinsic, irreducible background. Diphoton production is the dominant background in our high mass signal region.
- γ+jets: A jet from γ+jets production can be misidentified as a photon when an outgoing quark undergoes final state radiation or when the quark or gluon of the jet fragments to leading π^0 or η meson, then decaying to a pair of photons which may be indistinguishable at high p_T.

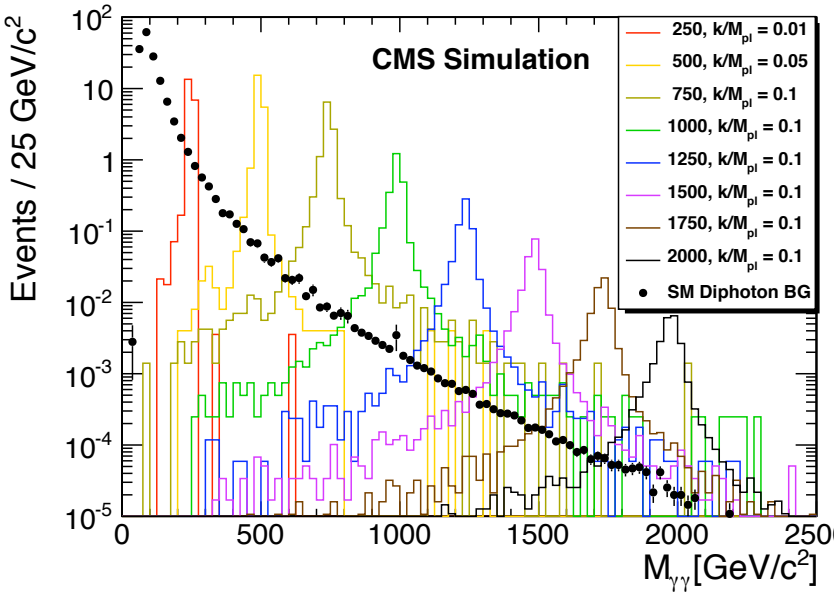

Figure 1: MC signal Randall-Sundrum diphoton invariant mass distribution, after selection and scaled to 36.1 pb^{-1}. SM diphoton background contribution is overlaid in black dots.

- jets: Likewise, QCD dijet events can contribute to this final state when both jets are misidentified as photons.
- e^+e^-: Finally, Drell-Yan dielectron events can result in an apparent diphoton signature if the electron lose significant energy through bremsstrahlung, or if the electron track fails to be reconstructed. As the mis-indentification of electrons as photons after our strict isolation requirements is small, this background is negligible in our signal region.

The final background extrapolation in the limit setting procedure is done with a fit to the data distribution. However, we present background estimates to ensure that we understand the data $M_{\gamma\gamma}$ spectrum in terms of the known SM components, namely real diphoton events and "fake" photon signatures from misidentified jets, before proceeding with setting limits.

Contributions from events where one or both photons are fake are a large component of the diphoton final state. The jet-faking-photon rate cannot be estimated from simulation, because it is governed by rare cases of jet fragmentation, and there is no guarantee that the simulation describes these rare cases well enough. We therefore use a data-derived photon fake rate, which relates a control sample of "fake" objects (which are selected to be well-isolated and photon-like, but vetoing candidates which pass tight isolation or shower shape requirements) to "tight" photon candidates which pass the tight requirements described earlier. By weighting "fake" objects from our control sample with the fake rate, we estimate the number of hadronic jets which are misidentified as photons in our data sample. A 20% systematic uncertainty is assigned to this fake rate, which comes from two main sources: from the extraction of the real photon contribution to the numerator objects; and from the differences in the fake rate measured in different final states, which in turn arises from differences in the relative quark/gluon composition of the jets.

The contribution from events with two real photons is obtained from the diphoton MC, and needs to be added to these fake contributions to give the total background estimate for the final state. Based on previous experience at the Tevatron, we expect these leading-order PYTHIA

predictions for photon+jet and diphoton processes need to be scaled by a *K*-factor to account for higher-order contributions. As a conservative estimate, henceforth we apply a NLO *K*-factor of 1.3 ± 0.3 to the diphoton background MC estimate [19, 20]. The error covers the variation of the *K*-factor as a function of $M_{\gamma\gamma}$.

Figure 2 shows the $M_{\gamma\gamma}$ invariant mass distribution after the selection described earlier has been applied to the data. Overlaid in colored histograms are the background estimations from the data-driven method as described earlier. We see a yield of 475 diphoton candidate events in 36.1 pb^{-1}, with 12 events with diphoton invariant mass > 200 GeV$/c^2$. The highest mass pair has $M_{\gamma\gamma}$=432 GeV$/c^2$. We find no evidence for a high-mass diphoton resonance in this spectrum. Event displays for the highest-mass diphoton events are presented in Appendix A.

Table 1 shows the comparison of the yield from data and the expected background from the data driven technique described earlier. As described earlier, the statistical error is small compared to the large systematic errror ($\sim$ 20%). In addition, we quote a 23% error on the uncertainty of the *K*-factor applied to the diphoton cross section, as described earlier.

Sample	$0 < M_{\gamma\gamma} < 60$ GeV$/c^2$	$60 < M_{\gamma\gamma} < 200$ GeV$/c^2$	$200 < M_{\gamma\gamma} < 500$ GeV$/c^2$	$500 < M_{\gamma\gamma} < 1000$ GeV$/c^2$
Diphoton	0.6 $\pm$ 0.04 $\pm$ 0.1	148.0 $\pm$ 0.4 $\pm$ 34.2	6.1 $\pm$ 0.1 $\pm$ 1.4	0.27 $\pm$ 0.01 $\pm$ 0.06
QCD Jets	3.0 $\pm$ 0.3 $\pm$ 0.8	69.1 $\pm$ 1.4 $\pm$ 19.5	0.5 $\pm$ 0.04 $\pm$ 0.1	0.001 $\pm$ 0.001 $\pm$ 0.0003
γ+Jet	18.3 $\pm$ 4.3 $\pm$ 5.1	144.8 $\pm$ 7.1 $\pm$ 68.8	2.3 $\pm$ 0.5 $\pm$ 0.7	0.02 $\pm$ 0.02 $\pm$ 0.004
TOTAL	21.9 $\pm$ 4.4 $\pm$ 4.9	362.0 $\pm$ 7.2 $\pm$ 68.9	8.9 $\pm$ 0.5 $\pm$ 1.6	0.29 $\pm$ 0.03 $\pm$ 0.06
Data	35	428	12	0

Table 1: Number of diphoton candidates passing selection, for data-driven background estimation and raw data yield. The first error is statistical. The second error on the background estimates are systematic: the γ+jet and QCD dijets estimates have a $\sim$ 20% systematic uncertainty; the diphoton estimate has a 23% uncertainty from the *K*-factor of 1.3 applied.

In the absence of any significant resonance in the diphoton data, we set limits on the RS model parameters: the graviton mass M_1 and the coupling parameter $\tilde{k}$. As this is a search for a narrow resonance, we assume there is no signal contamination outside of the search window and we proceed to set limits by applying a fit to the data distribution to extrapolate the expected number of background events in a sliding mass window. We next describe the signal and background parametrization, and the model parameter limits obtained.

The signal is parametrized as a Crystal Ball + Gaussian function, and we compute a measure of the signal width, $\sigma_{\text{effective}}$, defined as the half-width of the narrowest mass interval containing 68% of the signal. The mass resolution varies from $\approx 1-2$%, depending on $\tilde{k}$. For optimum signal sensitivity, we find that the upper bound of the mass window extends to infinity, while the lower bound is set to be $5 \times \sigma_{\text{effective}}$ below the mass. The signal efficiency for this mass window definition is roughly 95%. Note that for the extrapolation of the limits, we apply a *K*-factor to account for NLO effects in the RS signal cross section. We use a *K*-factor of 1.3 ± 0.3 [19, 20]. We take the uncertainty on the *K*-factor as a theoretical uncertainty.

For the background parametrization, we use a function of the form: $e^{c_0+c_1\cdot x+c_2\cdot x^2+c_3\cdot x^3+c_4\cdot x^4}$. The shape of the background function is fixed with a fit to MC in the region $220-1000$ GeV$/c^2$. Then the background function is normalized using a data control region $100-220$ GeV$/c^2$; the region was selected to be high enough in $M_{\gamma\gamma}$ to avoid contamination from Z^0 decays and low enough to be outside of the signal region. The background function is then extrapolated into the signal region to estimate the background.

From the signal efficiency, background parametrization, and the observed data, a Bayesian

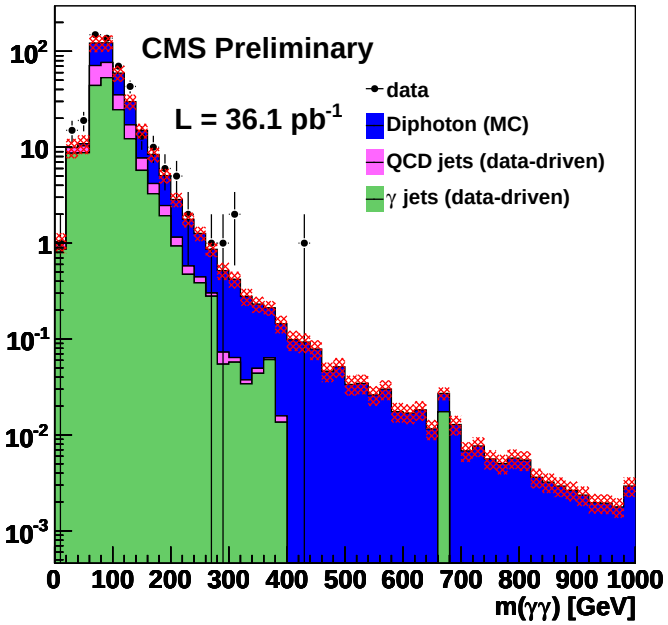

Figure 2: Diphoton invariant mass distribution after selection from 36.1 pb^{-1}, with data-driven background overlaid. Systematic uncertainty on background estimate is overlaid in red.

counting method is used to calculate 95% C.L. upper limits on the signal cross section times branching ratio ($\mathcal{B}$) in each mass window. In computing the limits, an 11% systematic error on the integrated luminosity is applied. In addition, we account for a 2% error on the signal efficiency, due to the difference between MC measured efficiency and data-driven efficiency from tag-and-probe. We also apply a 1.5% PDF uncertainty on the signal acceptance. To estimate the systematic error arising from the background shape, we vary the parameters of the exponential fit by $\pm 1\sigma$ and check the variation in expected background events. In addition, we cross-check the uncertainty due to the diphoton K-factor in the background shape, by varying the K-factor to 2.0 and taking the variation with respect to the results with $K = 1.3$ as the uncertainty. As a result, we estimate a total $\sim$ 10% uncertainty in the overall background shape due to the shape parameters and K-factor. A systematic uncertainty on the K-factor for the graviton signal is taken as a theoretical uncertainty and is not used in the limit setting. Since we are statistically limited in the high mass region, we find that the systematic errors have little effect on the final limits on the model parameters.

Figure 3 shows the 95% C.L. limit on the observed $\sigma \times \mathcal{B}$ compared to the theoretical graviton $\sigma \times \mathcal{B}$, as a function of the graviton mass, for various values of $\tilde{k}$. We then translate the upper limit on the cross section into lower limits on the graviton mass M_1. Figure 4 shows the limits in the M_1 vs $\tilde{k}$ plane. For $\tilde{k}$=0.01, 0.05, and 0.1, we exclude at the 95% confidence level graviton masses below 371, 731, and 945 GeV/c^2, respectively.

We note that limits on the large extra dimension scenario have also been placed in the diphoton final state, using the same selection as this analysis [21].

In conclusion, we report the results of the first search for Randall-Sundrum graviton production in the diphoton channel using data corresponding to an integrated luminosity of 36.1 $\text{pb}^{-1}$of pp collisions at $\sqrt{s} = 7$ TeV, collected by the CMS detector. We find no evidence for a resonance

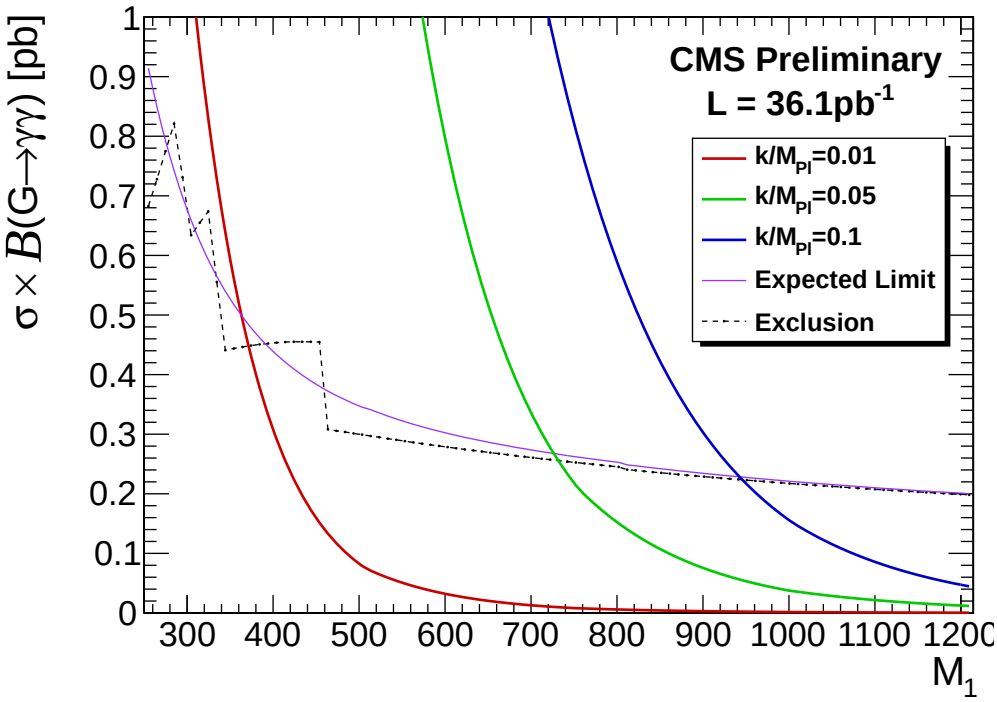

Figure 3: 95% limit on theoretical cross section times branching ratio for RS graviton prodution, as a function of the graviton mass M_1, for k/M_{Pl}=0.01 (red), 0.05 (green), 0.1 (blue). The expected limit is overlaid in a purple solid line, and the exclusion region is delineated by a dashed black line.

and set limits on the graviton mass and coupling parameters. For values of the coupling parameter ranging from 0.01 to 0.1, we find that at 95% confidence level, graviton masses below 371 to 945 GeV/$c^2$are excluded.

We thank the technical and administrative staff at CERN and other CMS Institutes, and acknowledge support from: FMSR (Austria); FNRS and FWO (Belgium); CNPq, CAPES, FAPERJ and FAPESP (Brazil); MES (Bulgaria); CERN; CAS, MST and NSFC (China); MST (Croatia); RPF (Cyprus); Academy of Sciences and NICPB (Estonia); Academy of Finland, ME and HIP (Finland); CEA and CNRS/IN2P3 (France); BMBF, DFG and HGF (Germany); GSRT and Leventis Foundation (Greece); OTKA and NKTH (Hungary); DAE and DST (India); IPM (Iran); SFI (Ireland); INFN (Italy); KICOS (Korea); CINVESTAV, CONACYT, SEP and UASLP-FAI (Mexico); PAEC (Pakistan); SCSR (Poland); FCT (Portugal); JINR (Armenia, Belarus, Georgia, Ukraine, Uzbekistan); MST and MAE (Russia); MSD (Serbia); MCINN and CPAN (Spain); Swiss Funding Agencies (Switzerland); NSC (Taipei); TUBITAK and TAEK (Turkey); STFC (United Kingdom); DOE and NSF (USA).

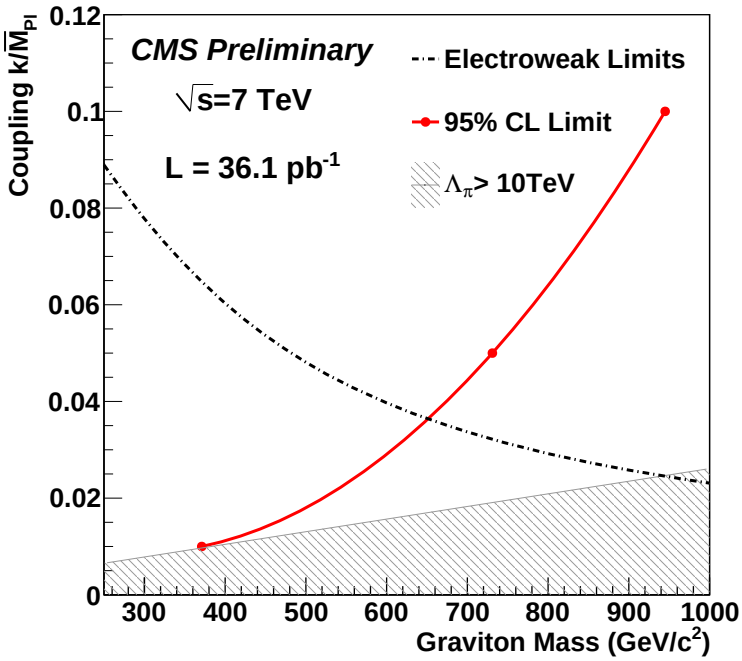

Figure 4: 95% C.L. limits obtained on the RS graviton mass for different values of the coupling parameter k/M_{Pl}. The area to the left of the red curve is excluded. The gray shaded region shows the area excluded for $\Lambda_\pi > 10$ TeV. The area below the dash-dotted line is excluded by precision electroweak data [22].

References

[1] N. Arkani-Hamed, S. Dimopoulos, and G. R. Dvali, "The hierarchy problem and new dimensions at a millimeter", *Phys. Lett.* **B429** (1998) 263–272, arXiv:hep-ph/9803315. doi:10.1016/S0370-2693(98)00466-3.

[2] I. Antoniadis, N. Arkani-Hamed, S. Dimopoulos et al., "New dimensions at a millimeter to a Fermi and superstrings at a TeV", *Phys. Lett.* **B436** (1998) 257–263, arXiv:hep-ph/9804398. doi:10.1016/S0370-2693(98)00860-0.

[3] L. Randall and R. Sundrum, "A large mass hierarchy from a small extra dimension", *Phys. Rev. Lett.* **83** (1999) 3370–3373, arXiv:hep-ph/9905221. doi:10.1103/PhysRevLett.83.3370.

[4] I. Antoniadis, "A Possible new dimension at a few TeV", *Phys. Lett.* **B246** (1990) 377–384. doi:10.1016/0370-2693(90)90617-F.

[5] I. Antoniadis, C. Munoz, and M. Quiros, "Dynamical supersymmetry breaking with a large internal dimension", *Nucl. Phys.* **B397** (1993) 515–538, arXiv:hep-ph/9211309. doi:10.1016/0550-3213(93)90184-Q.

[6] I. Antoniadis and K. Benakli, "Limits on extra dimensions in orbifold compactifications of superstrings", *Phys. Lett.* **B326** (1994) 69–78, arXiv:hep-th/9310151. doi:10.1016/0370-2693(94)91194-0.

[7] CDF Collaboration, "Search for Randall-Sundrum Gravitons in the Diphoton Channel at CDF", *Phys. Rev.* **D83** (2011) 011102, arXiv:1012.2795. doi:10.1103/PhysRevD.83.011102.

[8] The CDF Collaboration, "Search for New Dielectron Resonances and Randall-Sundrum Gravitons at the Collider Detector at Fermilab". http://www-cdf.fnal.gov/physics/exotic/r2a/20110214.gravitonee/index.html, 2011.

[9] The D0 Collaboration, "Search for Randall-Sundrum gravitons in the dielectron and diphoton final states with 5.4 fb-1 of data from ppbar collisions at sqrt(s)=1.96 TeV", *Phys. Rev. Lett.* **104** (2010) 241802, arXiv:1004.1826. doi:10.1103/PhysRevLett.104.241802.

[10] CMS Collaboration, "The CMS experiment at the CERN LHC", *JINST* **3** (2008) S08004. doi:10.1088/1748-0221/3/08/S08004.

[11] CMS Collaboration, "CMS physics: Technical design report",. CERN-LHCC-2006-001.

[12] CMS Collaboration, "CMS technical design report, volume II: Physics performance", *J. Phys.* **G34** (2007) 995–1579. doi:10.1088/0954-3899/34/6/S01.

[13] CMS Collaboration, "CMS Tracking Performance Results from early LHC Operation", *Eur. Phys. J.* **C70** (2010) 1165–1192, arXiv:1007.1988. doi:10.1140/epjc/s10052-010-1491-3.

[14] S. Agostinelli, J. Allison, K. Amako et al., "G4–a simulation toolkit", *Nuclear Instruments and Methods in Physics Research Section A: Accelerators, Spectrometers, Detectors and Associated Equipment* **506** (2003), no. 3, 250 – 303. doi:10.1016/S0168-9002(03)01368-8.

[15] T. Sjostrand, P. Eden, C. Friberg et al., "High-Energy-Physics Event Generation with PYTHIA 6.1", 2000.

[16] The CMS Collaboration, "Photon reconstruction and identification at $\sqrt{(s)} = 7$ TeV", *CMS Physics Analysis Summary* **2010/005** (2010).

[17] The CMS Collaboration, "Measuring Electron Efficiencies at CMS with Early Data", *CMS Physics Analysis Summary* **2007/001** (2007).

[18] The CMS Collaboration, "Isolated Photon Reconstruction and Identification at $\sqrt{(s)} = 7$ TeV", *CMS Physics Analysis Summary* **2010/006** (2010).

[19] M. C. Kumar, P. Mathews, V. Ravindran et al., "Diphoton signals in theories with large extra dimensions to NLO QCD at hadron colliders", *Phys. Lett.* **B672** (2009) 45–50, arXiv:0811.1670. doi:10.1016/j.physletb.2009.01.002.

[20] M. C. Kumar, P. Mathews, V. Ravindran et al., "Direct photon pair production at the LHC to order α_s in TeV scale gravity models", *Nucl. Phys.* **B818** (2009) 28–51, arXiv:0902.4894. doi:10.1016/j.nuclphysb.2009.03.022.

[21] CMS Collaboration, "Search for Large Extra Dimensions in the Diphoton Final State at the Large Hadron Collider", arXiv:1103.4279.

[22] H. Davoudiasl, J. L. Hewett, and T. G. Rizzo, "Experimental probes of localized gravity: On and off the wall", *Phys. Rev.* **D63** (2001) 075004, arXiv:hep-ph/0006041. doi:10.1103/PhysRevD.63.075004.

A Selected High-Mass Diphoton Events

In Figure 5 we show event displays for the highest-mass diphoton events observed in the data.

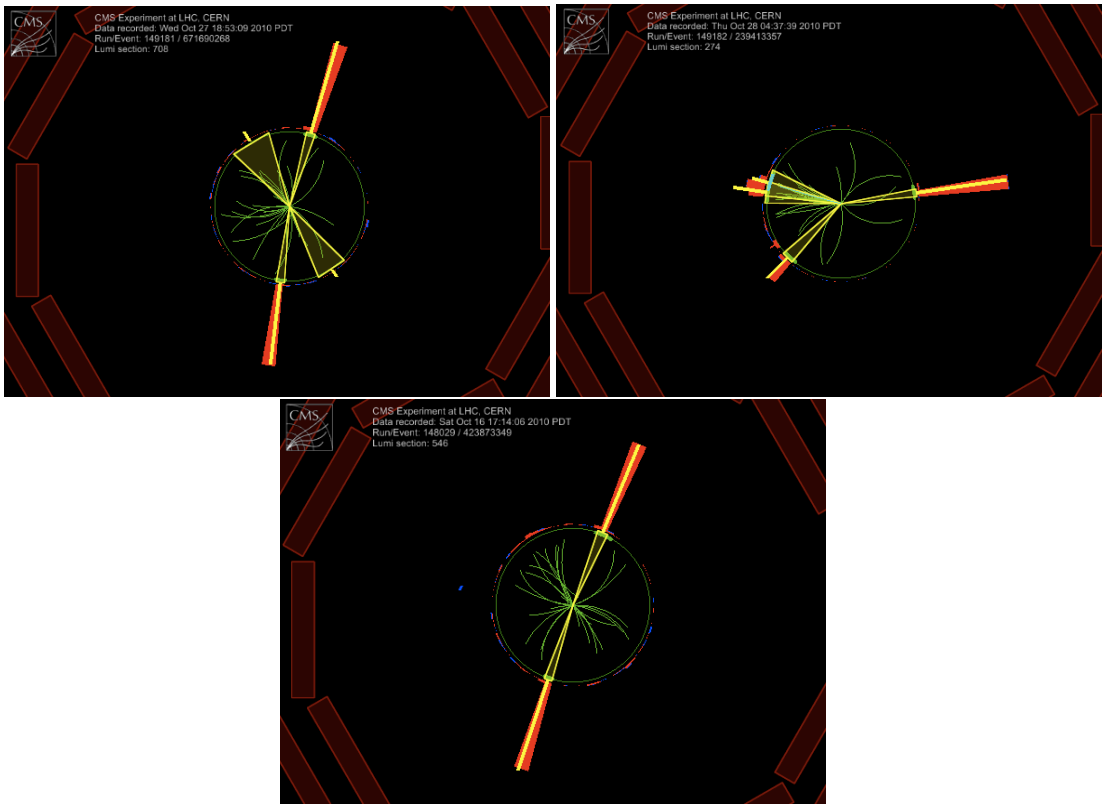

Figure 5: Event displays for the highest-mass diphoton events in the data

B Table of Yields

Table 2 summarizes the expected and actual event yields for signal MC, background from the fit to data, and data yields for a sample of graviton mass and $\tilde{k}$ values.

$\tilde{k}$	M_1	Signal Efficiency	Expected Signal	Expected Background	Data
0.01	250	0.251	18.3	6.49	5
0.01	500	0.309	0.788	0.285	0
0.01	750	0.358	0.101	0.0522	0
0.01	1000	0.411	0.0211	0.0165	0
0.01	1250	0.458	0.00572	0.00604	0
0.01	1500	0.498	0.00176	0.00269	0
0.05	500	0.306	19.5	0.278	0
0.05	750	0.359	2.53	0.0541	0
0.05	1000	0.411	0.534	0.0173	0
0.05	1250	0.462	0.145	0.00629	0
0.05	1500	0.497	0.044	0.00282	0
0.05	1750	0.531	0.0148	0.00174	0
0.1	750	0.365	10.2	0.0637	0
0.1	1000	0.417	2.14	0.0205	0
0.1	1250	0.464	0.567	0.0076	0
0.1	1500	0.504	0.177	0.00328	0
0.1	1750	0.535	0.0591	0.00192	0
0.1	1750	0.56	0.021	0.00145	0

Table 2: Signal efficiency and expected number of signal events from simulation, expected background events, and raw yields, in 36 $pb^{-1}$of data.